Nonlinear development of two-layer Couette–Poiseuille flow in the presence of surfactant

Andrew P. Bassom,[1] M. G. Blyth,[2,a)] and D. T. Papageorgiou[3]
[1]*School of Mathematics and Statistics, University of Western Australia, Crawley 6009, Australia*
[2]*School of Mathematics, University of East Anglia, Norwich NR4 7TJ, United Kingdom*
[3]*Department of Mathematics, Imperial College London, London SW7 2AZ, United Kingdom*

(Received 11 January 2010; accepted 10 August 2010; published online 12 October 2010)

The two-dimensional nonlinear evolution of the interface between two superposed layers of viscous fluid moving in a channel in the presence of an insoluble surfactant is examined. A pair of coupled weakly nonlinear equations is derived describing the interfacial and surfactant dynamics when one of the two fluid layers is very thin in comparison to the other. In contrast to previous work, the dynamics in the thin film are coupled to the dynamics in the thicker layer through a nonlocal integral term. For asymptotically small Reynolds number, the flow in the thicker layer is governed by the Stokes equations. A linearized analysis confirms the linear instability identified by previous workers and it is proven that the film flow is linearly unstable if the undisturbed surfactant concentration exceeds a threshold value. Numerical simulations of the weakly nonlinear equations reveal the existence of finite amplitude traveling-wave solutions. For order one Reynolds number, the flow in the thicker layer is governed by the linearized Navier–Stokes equations. In this case the weakly nonlinear film dynamics are more complex and include the possibility of periodic traveling-waves and chaotic flow. © *2010 American Institute of Physics*. [doi:10.1063/1.3488226]

I. INTRODUCTION

Yih[1] demonstrated that two superposed fluid layers confined in a channel and driven by the motion of one of the walls and/or by an axial pressure gradient are susceptible to an interfacial instability associated with the viscosity contrast between the fluids. Using a perturbation analysis, Yih showed that the flow may be linearly unstable to long wavelength disturbances for arbitrarily small but nonzero values of the Reynolds number depending on the viscosity ratio and the thickness ratio of the two fluid layers. Interestingly, the confining channel walls play a key role in determining the nature of the instability. Hooper and Boyd[2] pointed out that for two semi-infinite fluid layers, the flow is unstable to short wavelength perturbations in the absence of surface tension, and that surface tension exerts a stabilizing influence. Moreover, Hooper[3] showed that when the upper wall of the channel is removed, the growth rate of long wavelength perturbations is larger than that calculated by Yih, suggesting that the upper wall has a stabilizing influence on the flow. Hooper's results indicate that the flow is stable if the thin lower layer contains the less viscous fluid. Hooper and Grimshaw[4] developed Yih's analysis to include weak nonlinearity and derived a Kuramoto–Sivashinsky evolution equation describing the spatiotemporal development of interfacial perturbations in the strong surface tension limit. Charru and Fabre[5] carried out a similar analysis, but with a slightly weakened assumption on the size of the surface tension and noted that in the case of Couette flow, a stable flow can become unstable when the Reynolds number is lowered, suggesting that inertia has a stabilizing effect. In both sets of analyses, the results are consistent with Yih's results for small-amplitude perturbations.

Frenkel and Halpern[6,7] and Halpern and Frenkel[7] demonstrated for the first time that the flow studied by Yih is unstable at zero Reynolds number when the interface is contaminated with an insoluble surfactant. The instability depends crucially on the presence of surfactant on the interface and on the basic shearing motion between the fluids. In the absence of one or other of these factors, the instability does not arise. Blyth and Pozrikidis[8] confirmed Frenkel and Halpern's predictions and performed nonlinear calculations in the zero Reynolds number limit using the boundary integral method. They found evidence of saturated solutions corresponding to traveling-waves on restricted periodic domain sizes. Wei[9] provided a discussion of the underlying instability mechanism taken from the viewpoint of vorticity. The role of inertia on the interfacial instability was investigated by Pozrikidis[10] and Blyth and Pozrikidis[11] for perturbations of arbitrary wavelength at arbitrary Reynolds number and by Frenkel and Halpern[12] for long wavelength perturbations. The results showed that inertia tends to widen the range of unstable wavenumbers.

Frenkel and Halpern[13] pointed out that the saturated traveling-wave solutions predicted by Blyth and Pozrikidis[8] would most likely disappear when the same calculations are repeated on much wider domains, permitting the inclusion of many fundamental wave periods. Making the simplifying assumption of a semi-infinite upper fluid and working on the basis of the lubrication approximation, Frenkel and Halpern derived a set of coupled, nonlinear equations describing the deformation of the interface and the interfacial surfactant concentration. The evolution equations depend on the basic flow quantities, including the basic shear rate at the interface

a)Electronic mail: m.blyth@uea.ac.uk.

and the longitudinal pressure gradient driving the basic flow, but do not depend on the perturbations in the upper, semi-infinite layer. The same authors derived a reduced set of weakly nonlinear equations on the assumption of small-amplitude disturbances. Numerical solutions of the fully nonlinear evolution equations revealed that, as the domain size is lengthened, shortwave saturated solutions become unstable to small wavenumber perturbations and ultimately evolve into pulselike traveling-wave solutions of long wavelength. Notably, they observed that in contrast to other instabilities involving two fluid layers, the saturation of the linearly unstable waves cannot occur at small-amplitude, which implies that the weakly nonlinear forms of the equations are incapable of capturing the long-term dynamics. In related work, Halpern and Frenkel[14] derived a modified form of the weakly nonlinear equations valid for perturbations with near-marginal wavelength. They noted that the extra nonlinear terms in the modified equations presented the possibility of small-amplitude saturated waves and confirmed this prediction through a Stuart–Landau type analysis. Finally, they showed that the small-amplitude waves are unstable to long-wave perturbations which invariably result in large amplitude saturated solutions in numerical simulations.

In this paper, we revisit the problem of contaminated two-layer flow in a channel when the lower layer is thin in comparison to the upper layer. The novelty of our work lies in the derivation of a weakly nonlinear equation for the interfacial shape which accounts for a coupling between the dynamics in the thin film and those in the upper layer. The cornerstone of the analysis is the theory developed by Papageorgiou *et al.*[15] for core-annular flow in the limit of a thin outer layer, and later extended by Kas-Danouche *et al.*[16] to include an insoluble surfactant. The dynamics of the annular film were described by a nonlinear evolution equation which is coupled to the motion in the core region through a nonlocal integral term. Further discussion of fluid-core coupling through a nonlocal term may be found in Joseph and Renardy.[17] Kas-Danouche *et al.*[16] retained Marangoni effects in the leading order dynamics by assuming a small base concentration of surfactant. Here we show that a similar analysis may be carried out for the presently considered channel problem, and a weakly nonlinear evolution equation may be derived with a nonlocal term coupling the dynamics in the thin lower layer to those in the overlying fluid. At zero Reynolds number, a key difference between the two problems is the absence of a second spatial derivative of the thin film thickness in the interfacial evolution equation. This difference may be traced to the destabilizing circumferential curvature term present in axisymmetry. As a consequence, the interfacial dynamics at zero Reynolds number is considerably simpler for the channel problem than for its core-annular counterpart. More complex dynamics, including periodic traveling-waves and chaotic solutions, arise in the case of channel flow at nonzero Reynolds number when inertia is present.

In Sec. II the mathematical problem is formulated and the pertinent asymptotic scalings are presented. In Sec. III a system of two coupled weakly nonlinear equations for the evolution of the film thickness and surfactant concentration is derived on the assumption of Stokes flow and numerical solutions are presented. The modified forms of the equations for nonzero Reynolds number are derived in Sec. IV and solved numerically. In Sec. V we summarize our findings.

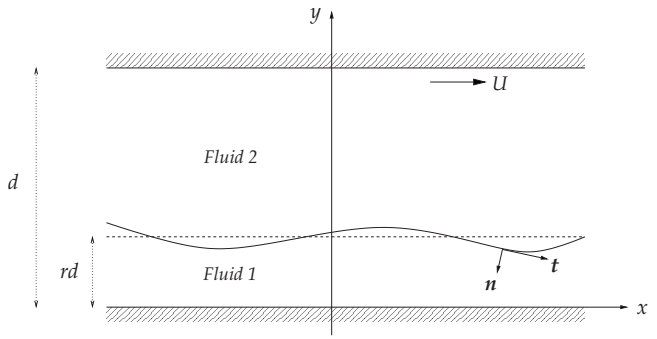

FIG. 1. Sketch of the flow configuration consisting of two superposed viscous fluids in a channel. The motion is driven by a pressure gradient and/or by the motion of the upper wall at speed U. In the analysis, the lower layer is assumed to be very thin.

II. MATHEMATICAL MODEL

We consider the flow of two superposed viscous fluid layers in a channel, when the flow is driven by a pressure gradient or by the motion of the upper wall of the channel, or by a combination of both. The two fluids have the same density but generally different viscosities. Referring to the sketch in Fig. 1, the lower fluid is labeled fluid 1 and the upper fluid is labeled fluid 2. The lower wall of the channel lies at $y=0$ and the upper wall lies at $y=d$. The interface between the two fluids is populated by an insoluble surfactant which is free to move along the interface, and whose effect is to lower the surface tension by an amount depending on the local concentration of surfactant. In the unperturbed configuration the interface between the two fluids is flat and is located at $y=rd$, where $0<r<1$. Our aim is to analyze the flow when r is small and the lower fluid layer is thin in comparison to the channel width. Equivalently, since gravitational effects are neglected, our analysis applies for r close to unity when the upper layer is thin in comparison to the lower layer (this can be achieved by changing the frame of reference).

We nondimensionalize using the channel width d for the length scale, the velocity of the upper wall in the x direction, U, as the velocity scale, ρU^2 as the pressure scale, and d/U as the time scale. The surface tension is nondimensionalized using the value prevailing for a clean interface in the absence of surfactant, γ_c. The surfactant concentration is nondimensionalized using the maximum packing concentration of surfactant, Γ_∞. The flow in the two fluids is governed by the Navier–Stokes equations, which in dimensionless variables are written as

$$u_{jt}+u_j u_{jx}+v_j u_{jy}=-p_{jx}+\frac{1}{R_j}(u_{jxx}+u_{jyy}), \tag{1a}$$

$$v_{jt}+u_j v_{jx}+v_j v_{jy}=-p_{jy}+\frac{1}{R_j}(v_{jxx}+v_{jyy}), \tag{1b}$$

$$u_{jx} + v_{jy} = 0, \tag{1c}$$

where t is the dimensionless time, u_j, v_j are the x and y velocity components, respectively, and p_j is the pressure in fluid $j=1,2$. The Reynolds numbers in the two fluids are given by

$$R_1 = \frac{\rho U d}{\mu_1}, \quad R_2 = \frac{\rho U d}{\mu_2} = \frac{R_1}{m}, \tag{2}$$

where ρ is the common density of the fluids, μ_j is the viscosity of fluid $j=1,2$, and $m=\mu_2/\mu_1$ is the viscosity ratio.

In the basic, unperturbed flow, the fluid motion is unidirectional in the x direction and the interface between the fluids is flat and located at $y=r$. Using an overbar to indicate the basic state, the unperturbed flow velocities and pressure are given by

$$\bar{u}_1 = -a_1 y^2 + b_1 y, \quad \bar{v}_1 = 0, \tag{3a}$$

$$\bar{u}_2 = -a_2 y^2 + b_2 y + c_2, \quad \bar{v}_2 = 0, \tag{3b}$$

$$\bar{p}_1 = \bar{p}_2 = -(Gd/\rho U^2)x = -(2a_1/R_1)x, \tag{3c}$$

where $G>0$ is the constant imposed axial pressure gradient, and the dimensionless coefficients

$$a_1 = \frac{Gd^2}{2\mu_1 U}, \quad b_1 = \frac{a_1[r^2(m-1)+1]+m}{r(m-1)+1}, \tag{4}$$

$$c_2 = \left(1 - \frac{1}{m}\right)\frac{a_1 r(1-r) + rm}{r(m-1)+1},$$

and $a_2=a_1/m$ and $b_2=b_1/m$.

Our interest lies in following the development of the initially flat interface when the flow is disturbed from the basic state so that its new position is given by $y=S(x,t)$, which, in general, is a function of time and space. In the presence of such a disturbance, the surfactant concentration at a point on the interface will be altered from its basic uniform reference value according to a convection-diffusion equation (Wong *et al.*;[18] Li and Pozrikidis[19]), which in the present context is most conveniently written in the form provided by Halpern and Frenkel,[7]

$$[(1+S_x^2)^{1/2}\Gamma]_t + [(1+S_x^2)^{1/2}u_s\Gamma]_x = \frac{1}{\mathrm{Pe}}\left[\frac{\Gamma_x}{(1+S_x^2)^{1/2}}\right]_x, \tag{5}$$

where $u_s \equiv u_1(x,S) = u_2(x,S)$ is the horizontal velocity component at the interface and the Péclet number $P_e = Ud/D_s$ for surfactant diffusivity D_s. Assuming that the surfactant is present in only a dilute concentration, the interfacial surface tension is modified locally according to the linear Gibbs' isotherm which, written in the present nondimensional variables, is given by

$$\gamma = 1 - \beta\Gamma, \tag{6}$$

where the sensitivity of the interfacial tension to changes in the surfactant concentration is encapsulated in the parameter $\beta = RT\Gamma_\infty/\gamma_c$, where R is the universal gas constant and T is the absolute temperature. Note that linear law (6) is consistent with the perturbation scheme to be introduced below and would arise in the ensuing analysis if a nonlinear equation of state is used. For clarity, we proceed with the linearized isotherm.

At the interface, $y=S(x,t)$, the balance of normal and tangential stress requires that

$$(\boldsymbol{\sigma}_1 - \boldsymbol{\sigma}_2)\cdot\mathbf{n} = \kappa\gamma\mathbf{n} - \frac{\partial\gamma}{\partial l}\mathbf{t}, \tag{7}$$

where $\mathbf{n}$ is the unit normal pointing into fluid 1 as shown in Fig. 1, $\boldsymbol{\sigma}_j$ is the stress tensor in fluid j, and l measures increasing arc length along the interface in the direction of the unit tangent $\mathbf{t}$. The curvature κ is taken to be positive when the interface is concave upward and is given by the formula

$$\kappa = \frac{S_{xx}}{(1+S_x)^{3/2}}. \tag{8}$$

The normal stress jump at the interface is obtained by taking the dot product of (7) with the unit normal $\mathbf{n}$ and is given by

$$\left\{p_j(1+S_x^2) - \frac{2}{R_j}[u_{jx}S_x^2 - (u_{jy}+v_{jx})S_x + v_{jy}]\right\}_2^1 = -\frac{J(1-\beta\Gamma)}{R_1^2}\frac{S_{xx}}{(1+S_x^2)^{1/2}}, \tag{9}$$

where the notation $[\bullet_j]_2^1$ means $\bullet_1 - \bullet_2$, and we have introduced the dimensionless parameter $J=\rho\gamma_c d/\mu_1^2$ (Chandrasekhar[20]). The tangential stress jump is obtained by taking the dot product of (7) with the unit tangent $\mathbf{t}$ and is given by

$$[4m_j S_x u_{jx} + m_j(u_{jy}+v_{jx})(S_x^2-1)]_2^1 = \frac{\beta\Gamma_x}{\mathrm{Ca}}(1+S_x^2)^{1/2}, \tag{10}$$

where $m_1=1$ and $m_2=m$, and where the capillary number is defined as $\mathrm{Ca}=\mu_1 U/\gamma_c = R_1/J$.

In the ensuing analysis, we will assume that the lower layer, henceforth termed the film, is thin in comparison to the upper layer, and write $r=\epsilon$, where $\epsilon \ll 1$. Working under this assumption, our specific goal is to derive at a weakly nonlinear evolution equation for the film thickness. We assume that the interface undergoes a small perturbation so that

$$S(x,t) = \epsilon\eta(x,t), \quad \eta = 1 + \delta_1 H(x,t), \tag{11}$$

where $\delta_1 = \delta_1(\epsilon)$ is a small parameter depending on the size of ϵ. The surfactant concentration is perturbed so that $\Gamma(x,t) = \Gamma_0 + \delta_2\Gamma'$, where $\delta_2 = \delta_2(\epsilon)$ is a parameter whose size is to be determined. Our aim is to choose δ_1 and δ_2 to ensure a nonlinear evolution equation for the film thickness perturbation, $H(x,t)$, coupled to the fluid dynamics of the upper layer at leading order in the limit $\epsilon \to 0$. To this end, the asymptotic size of δ_1 is determined using a scaling analysis which very closely follows that presented by Kas-Danouche *et al.*[16] For this reason the specific details are omitted and we present the final asymptotic expansions directly. As in Kas-Danouche *et al.*[16] we arrive at the following key scalings:

$$m = O(1), \quad m - 1 = O(1), \quad \delta_1 = O(\epsilon), \quad \mathrm{Ca} = O(\epsilon),$$
$$\Gamma_0 = O(\delta_2), \quad \beta = O(\epsilon^3 \delta_2^{-1}), \quad \mathrm{Pe} = O(\epsilon^{-2}). \tag{12}$$

It is the scaling $\mathrm{Ca}=O(\epsilon)$ in Eq. (12) which is crucial in producing weakly nonlinear dynamics. If the scale $\mathrm{Ca}=O(\epsilon^2)$ is adopted instead, linear dynamics are obtained; this corresponds to the scaling chosen by Wei and Rumschitzki[21] for the core-annular problem. The scaling $\mathrm{Ca}=O(\epsilon)$, which was identified by Papageorgiou *et al.*[15] for the core-annular problem, yields nonlinear dynamics by first removing the linear convective term which appears in the interfacial evolution equation using a Galilean transformation. When surfactant is present, the difficulty in reaching nonlinear dynamics lies in simultaneously removing the linear convective terms from both the interfacial evolution equation and the surfactant evolution equation. This may be achieved under the scaling $\mathrm{Ca}=O(\epsilon)$ through a Galilean transformation provided that the surfactant perturbation is assumed to be of the same order of magnitude as the base level concentration (Kas-Danouche *et al.*[16]). It is important to note that the scaling for the surfactant concentration does not require δ_2 to be small; rather the size of δ_2 is arbitrary.

The dynamics in the upper fluid layer depend on the size of the Reynolds number. If $R_2=O(\epsilon)$ inertia is absent and the upper layer dynamics are governed by the linear equations of Stokes flow. If $R_2=O(1)$, inertia is present and the upper layer dynamics are controlled by the linearized Navier–Stokes equations. We will consider these two Reynolds number scalings individually in the next two sections and we will simulate the resulting dynamics.

III. STOKES FLOW IN THE UPPER LAYER: $R_2=O(\epsilon)$

We assume a small Reynolds number in both the upper layer and the film and write $R_2=\epsilon\lambda$, where $\lambda=O(1)$, so that $R_1=mR_2=\epsilon m\lambda$. Adopting scalings (12), we write

$$\mathrm{Ca} = \epsilon \mathrm{Ca}_0, \quad \beta = \epsilon^3 \delta_2^{-1} \beta_0, \quad \mathrm{Pe} = \epsilon^{-2} \mathrm{Pe}_0, \tag{13}$$

where the subscripted parameters are of order unity. The interface between the two fluids is located at

$$y = S(x,t) = \epsilon + \epsilon^2 H(x,t). \tag{14}$$

In the film, fluid 1, we introduce the new independent variable $\zeta=y/\epsilon$ and expand the flow variables about basic state (3) as follows:

$$u_1 = \bar{u}_1(y) + \epsilon^3 U_1(x,\zeta,t) + \cdots, \quad v_1 = \epsilon^4 V_1(x,\zeta,t) + \cdots, \tag{15a}$$

$$p_1 = \bar{p}_1 + P_1(x,\zeta,t) + \cdots, \tag{15b}$$

and we expand the surfactant concentration by writing

$$\Gamma = \delta_2 \tilde{\Gamma} + \cdots, \tag{16}$$

where we note that, as was mentioned above, it is not necessary to specify the size of δ_2. The expansions in Eq. (15) are motivated by the expected size of the film pressure perturbation suggested by normal stress balance (9) and by the requirement for a leading order balance between the pressure gradient term and the viscous term in the momentum equation. In addition, in the upper layer, fluid 2, we expand the flow variables as follows:

$$u_2 = \bar{u}_2(y) + \epsilon^2 U_2(x,y,t) + O(\epsilon^3), \tag{17a}$$
$$v_2 = \epsilon^2 V_2(x,y,t) + O(\epsilon^3),$$

$$p_2 = \bar{p}_2(y) + \epsilon P_2(x,y,t) + O(\epsilon^2). \tag{17b}$$

These expansions are motivated by the requirement of a continuous velocity field at the perturbed interface on noting that the jump in basic velocity field (3) at a point on the linearly perturbed interface is $O(\epsilon^2)$.

Substituting Eq. (15) into Navier–Stokes equations (1), we obtain the standard lubrication equations at leading order,

$$0 = -m\lambda P_{1x} + U_{1\zeta\zeta}, \tag{18a}$$

$$U_{1x} + V_{1\zeta} = 0, \tag{18b}$$

where $P_1=P_1(x,t)$. Substituting expansions (15) into normal stress balance (9), we find the leading order normal stress balance at the interface,

$$P_1 = -\frac{1}{m\mathrm{Ca}_0\lambda} H_{xx}. \tag{19}$$

Substituting Eq. (15) into tangential stress balance (10), we obtain the leading order tangential stress balance at the interface,

$$-U_{1\zeta}|_{\zeta=1} + m(U_{2y} + V_{2x})_{y=0} = \frac{\beta_0}{\mathrm{Ca}_0} \tilde{\Gamma}_x. \tag{20}$$

Integrating Eqs. (18a) and (18b) across the film and applying Eqs. (19) and (20), we obtain the following expression for the vertical velocity component at the interface:

$$V_1|_{\zeta=1} = -\frac{1}{3}\frac{1}{\mathrm{Ca}_0} H_{xxxx} + \frac{1}{2}\frac{\beta_0}{\mathrm{Ca}_0}\tilde{\Gamma}_{xx} - \frac{m}{2} T|_{y=0}, \tag{21}$$

where $T(x,y)=U_{2xy}+V_{2xx}$ and is found by solving the problem in the upper layer.

The kinematic condition requires that $v_1=S_t+u_1S_x$, at interface (14). Substituting expansions (15), we find

$$\epsilon^4 V_1|_{\zeta=1} = \epsilon^2 H_t + [\bar{u}_1(\epsilon) + \epsilon^2(a_1+m)H + \epsilon^3 U_1|_{\zeta=1}]\epsilon^2 H_x + \cdots, \tag{22}$$

where we have used the fact that $\bar{u}_1(S)=\bar{u}_1(\epsilon)+\epsilon^2(a_1+m)H + O(\epsilon^3)$. Introducing the Galilean transformation,

$$z = x - \bar{u}_1(\epsilon)t, \quad \tau = \epsilon^2 t, \tag{23}$$

in order to remove the term proportional to H_x, at leading order (22) reduces to

$$H_\tau + (a_1+m)HH_z = V_1|_{\zeta=1}. \tag{24}$$

Substituting expansions (14), (15a), (15b), and (16) into surfactant transport equation (5), making Galilean transformation (23) and retaining terms at leading order, we obtain

$$\tilde{\Gamma}_\tau + (a_1+m)(H\tilde{\Gamma})_z = \frac{1}{\mathrm{Pe}_0}\tilde{\Gamma}_{zz}. \tag{25}$$

In the upper layer, substituting Eq. (17) into Navier–Stokes equations (1), we obtain at leading order

$$0 = -\lambda P_{2x} + U_{2xx} + U_{2yy}, \tag{26a}$$

$$0 = -\lambda P_{2y} + V_{2xx} + V_{2yy}, \tag{26b}$$

$$U_{2x} + V_{2y} = 0. \tag{26c}$$

Introducing a streamfunction ψ, defined so that $U_2=\psi_y$ and $V_2=-\psi_x$, Eq. (26) reduces to the biharmonic equation $\nabla^4\psi=0$. We take a Fourier transform in x and integrate to obtain the general solution,

$$\psi^* = A_1 \sinh ky + A_2 \cosh ky + A_3 ky \sinh ky + A_4 ky \cosh ky, \tag{27}$$

where the A_i, $i=1,\ldots,4$ are functions of k and time and an asterisk superscript here and in the sequel indicates a Fourier transform. At the upper wall, we require that

$$\psi^* = \psi_y^* = 0, \tag{28}$$

at $y=1$. Continuity of velocity at the interface demands that $u_1=u_2$ and $v_1=v_2$ at $y=S(x,t)$. Substituting expansions (15) and (17) and then taking the Fourier transform, we obtain at leading order

$$\psi^* = 0, \quad \psi_y^* = \frac{1}{m}(m-1)(a_1+m)H^*, \tag{29}$$

at $y=0$. The four conditions in Eqs. (28) and (29) fix the constants A_i and determine the upper layer solution on completing the inverse Fourier transform. In particular, we find that

$$T|_{y=0} = \frac{\mathrm{i}}{\pi m}(1-m)(a_1+m)\int_{-\infty}^{\infty} N(k)H^*(k)\mathrm{e}^{\mathrm{i}kx}\mathrm{d}k, \tag{30}$$

where

$$N(k) = k^2\left(\frac{k-\cosh k \sinh k}{1+k^2-\cosh^2 k}\right). \tag{31}$$

The expression for T in Eq. (30) may now be substituted into Eq. (21), and the result into Eq. (24) to produce the desired weakly nonlinear evolution equation for the film thickness, $H(x,t)$. On making the transformation,

$$H \to \frac{1}{3(a_1+m)\mathrm{Ca}_0}H, \quad \tau \to 3\mathrm{Ca}_0\tau,$$
$$\tilde{\Gamma} \to \frac{2}{9(a_1+m)\mathrm{Ca}_0\beta_0}\tilde{\Gamma}, \tag{32}$$

the evolution equation reduces to its canonical form given by

$$H_\tau + HH_z + H_{zzzz} + \mathrm{i}\Lambda\int_{-\infty}^{\infty} N(k)\int_{-\infty}^{\infty} H(\tilde{z},\tau)\mathrm{e}^{\mathrm{i}k(z-\tilde{z})}\mathrm{d}\tilde{z}\mathrm{d}k - \tilde{\Gamma}_{zz} = 0, \tag{33}$$

and surfactant transport equation (25) reduces to its canonical form,

$$\tilde{\Gamma}_\tau + (H\tilde{\Gamma})_z = \eta\tilde{\Gamma}_{zz}, \tag{34}$$

where

$$\Lambda = \frac{3}{2\pi}\mathrm{Ca}_0(1-m)(a_1+m), \quad \eta = \frac{3\mathrm{Ca}_0}{\mathrm{Pe}_0}. \tag{35}$$

Note that Λ is positive if the upper fluid is less viscous than the film, and negative otherwise. We note that, on making the transformation $H\to -H$ and $z\to -z$, the sign on the surfactant term in Eq. (33) switches, while all of the terms in Eq. (34) remain the same. This establishes consistency with the evolution equations derived by Kas-Danouche *et al.*[16] for core-annular flow wherein a plus sign precedes the surfactant term in the interface evolution equation [see Eq. (4.2) of their paper].

Working on the basis of the lubrication approximation, Frenkel and Halpern[13] and Halpern and Frenkel[14] derived a set of nonlinear evolution equations for the film thickness and the surfactant concentration [see Eqs. (11) and (12) of Ref. 13 or, equivalently, (2.14) and (2.15) of Ref. 14]. Their equations are valid for interfacial disturbances and surfactant concentration disturbances both of which are not small in comparison to their basic state values. If we assume that the interfacial disturbance is indeed small (but the surfactant concentration disturbance is not), one can show that Eqs. (11) and (12) of Ref. 13 reduce to our Eqs. (33) and (34) for the uncoupled case $\Lambda=0$ and for $\eta=0$ when C is small.[22] However, it is worth emphasizing the differences between the present set of weakly nonlinear evolution equations (33) and (34) and those given as Eqs. (13) and (14) of Frenkel and Halpern.[13] The latter set of equations assume that both the interfacial and the surfactant concentration perturbations are small. In contrast, our weakly nonlinear equations are predicated on the assumption that only the interfacial perturbation is small but the surfactant perturbation is of the same order of magnitude as the base level concentration.

Following Smyrlis and Papageorgiou,[23] we consider a localization of evolution equation (33) obtained by replacing $N(k)$ by the first few terms of its Maclaurin expansion for small k. Specifically, we use the approximation

$$N(k) \approx 2k + \tfrac{2}{15}k^3. \tag{36}$$

Substituting Eq. (36) into Eq. (33), we obtain the localized form,

$$H_\tau + HH_z + H_{zzzz} + 2\Lambda\left(H_z - \tfrac{1}{15}H_{zzz}\right) - \tilde{\Gamma}_{zz} = 0. \tag{37}$$

which is to be solved in conjunction with Eq. (34). It was shown numerically by Smyrlis and Papageorgiou[23] that solutions of the localized and nonlocal systems are almost identical for a wide range of parameters and dynamical behaviors (e.g., traveling-waves, time-periodic solutions).

A. Linear stability analysis

To investigate the linear stability of the flow, we perturb about the basic state with $H=0$ and $\tilde{\Gamma}=\tilde{\Gamma}_0$, say, and write

$$H = Ae^{ikz+\sigma t} + \text{c.c.}, \quad \tilde{\Gamma} = \tilde{\Gamma}_0 + Be^{ikz+\sigma t} + \text{c.c.}, \tag{38}$$

where the wavenumber k is real, σ is the complex growth rate, c.c. denotes complex conjugate, and the complex constants A and B are both small. Substituting Eq. (38) into Eq. (33) we derive the dispersion relation

$$\sigma^2 + [k^4 + i\Lambda N(k) + \eta k^2]\sigma + [\eta k^6 + i\eta\Lambda k^2 N(k) - ik^3\tilde{\Gamma}_0] = 0. \tag{39}$$

Since this is a quadratic equation for σ, there are two normal modes, whose growth rates are given by $s=\text{Re}(\sigma)$, where Re denotes the real part. Yih[1] showed that, for a clean interface with no surfactant, the flow is linearly stable at zero Reynolds number. Frenkel and Halpern[6] demonstrated that the flow becomes unstable in the presence of surfactant with zero diffusivity provided that the interfacial shear associated with the basic flow is nonzero. Naturally, both of these observations should hold in the presently considered thin film limit. To discuss the stability properties, we consider first the case with no coupling between the film and upper layer corresponding to $\Lambda=0$. For small wavenumber k we find

$$s_{1,2} = \pm\left(\frac{\tilde{\Gamma}_0}{2}\right)^{1/2} k^{3/2} - \frac{\eta}{2}k^2 + \cdots, \tag{40}$$

where the plus sign applies for s_1 and the minus sign for s_2. In the absence of surfactant diffusivity, $\eta=0$, Eq. (40) coincides with Frenkel and Halpern's[6] result for the case $n=\infty$ (their notation) in their Table I. When $\tilde{\Gamma}_0=0$ and there is no surfactant in the flow, Eq. (40) indicates that the flow is stable. This underscores a key difference between the present two-dimensional analysis and the axisymmetric work carried out by Kas-Danouche *et al.*[16] for core-annular flow. In the latter case, the effect of surface tension combined with the azimuthal curvature of the flow configuration contributes an unstable mode which persists even in the absence of surfactant.

In Fig. 2(a) we show a stability graph for the case $\Lambda=0$, $\tilde{\Gamma}_0=1$, and $\eta=1$. The graph confirms the instability predicted by small wavenumber expansion (40) and shows that perturbation waves are stabilized above a cutoff value. For the case considered in the figure, the maximum growth rate $s_1=0.103$ occurs at $k=0.51$ and the cutoff wavenumber at which $s_1=0$ occurs at $k=0.79$. For completeness, we note that a large k expansion of the solutions to Eq. (39) predicts stability if $\eta>0$ but instability if $\eta=0$. However, the work of Frenkel and Halpern[13] indicates that a fourth-spatial derivative of H will appear in the next order correction to the surfactant transport equation, which will stabilize short waves; we have confirmed this to be the case by continuing our expansions to next order. In the present work, however, our concern is with solutions of model systems (33) and (34),

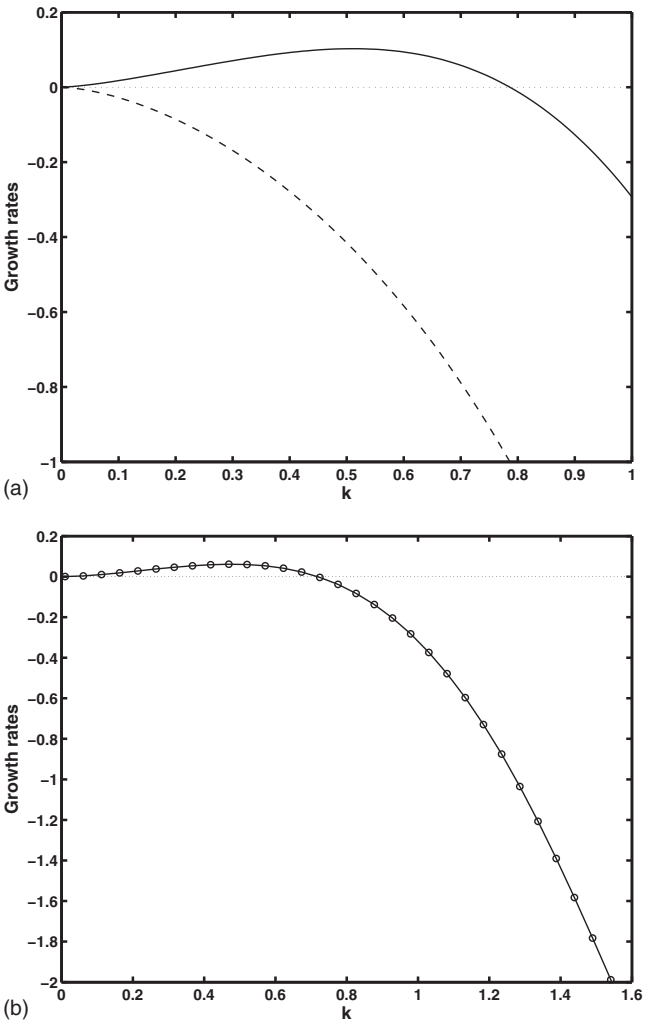

FIG. 2. (a) Growth rates s_1 (solid line) and s_2 (broken line) corresponding to solutions of Eq. (39) $\Lambda=0$, $\tilde{\Gamma}_0=1$, $\eta=1$. (b) The dominant growth rate s_1 for nonlocal equation (33) (solid line) and localized equation (37) (circles) for the case $\Lambda=0.25, \tilde{\Gamma}_0=1$, $\eta=1$.

and we do not claim that this accurately represents the short-wave behavior which would be identified from a short-wave expansion of the full problem.

When $\Lambda>0$, so that $m<1$ and the film is more viscous than the upper layer, we find for small k,

$$s_1 = \frac{(\tilde{\Gamma}_0 - 2\eta\Lambda)}{2\Lambda}k^2 + O(k^3), \quad s_2 = -\frac{\tilde{\Gamma}_0}{2\Lambda}k^2 + O(k^3), \tag{41}$$

for the two growth rates. It would appear, therefore, that the second normal mode with growth rate s_2 is stable and that the first normal mode with growth rate s_1 is stable to short wavelength perturbations, but unstable to long wavelength perturbations provided that

$$\tilde{\Gamma}_0 > 2\eta\Lambda. \tag{42}$$

In the absence of coupling between the film and the upper layer, corresponding to the case $\Lambda=0$, the flow would appear to be stable if $\tilde{\Gamma}_0=0$ and unstable otherwise. A stability graph for the unstable case $\Lambda=0.25$, $\tilde{\Gamma}_0=1$, and $\eta=1$ is qualitatively the same as that shown in Fig. 2(a), but with the maxi-

mum growth rate $s_1=0.061$ occurring at $k=0.48$ and with the cutoff wavenumber $k=0.72$. In fact, it can be proven that Eq. (42) provides both a sufficient and a necessary condition for instability at small wavenumber with a cutoff wavenumber beyond which both modes are linearly stable. The proof, which may be found in the Appendix, makes use of the argument principle (e.g., Ablowitz and Fokas[24]) to show that when Eq. (42) is satisfied, one of the zeros of Eq. (39) lies in the left-hand complex plane and one of the zeros lies in the right-hand complex plane leading to instability. When Eq. (42) is violated, both zeros lie in the left-hand plane and the flow is linearly stable. We note that Blyth and Pozrikidis[8] briefly considered the effect of surfactant diffusivity on the linear flow stability and found that it has a stabilizing effect, in agreement with what is found here.

When $\Lambda<0$, so that $m>1$ and the upper layer is more viscous than the film, the formulas for the small k expansion are the same as Eq. (41). Accordingly, for small enough k, s_2 is positive for any nonzero value of the base surfactant level $\tilde{\Gamma}_0$ and the flow is unstable. Typical stability graphs look qualitatively similar to that shown in Fig. 2(a). By way of comparison with the previous results, we note that for the case $\Lambda=-0.25$, $\tilde{\Gamma}_0=1$, and $\eta=1$, the maximum growth rate is $s_1=0.050$ which occurs at $k=0.46$ and the cutoff wavenumber is $k=0.65$.

It is instructive to compare the previous results with the stability properties of the localized form of evolution equation (37) together with surfactant transport equation (34). For $\Lambda\neq 0$ the small k expansions are exactly the same as Eq. (41) to the order shown and, in fact, agree to a higher order than that shown. Figure 2 displays the growth rate s_1 for the unstable case $\Lambda=0.25$, $\tilde{\Gamma}_0=1$, $\eta=1$ obtained for the full nonlocal evolution equation with Eq. (31) used in Eq. (39), shown as a solid line, and for the localized equation with Eq. (36) used in Eq. (39), shown with circles. The difference between the two is imperceptible.

B. Weakly nonlinear calculations

We calculate nonlinear solutions on the periodic domain $z\in[-L,L]$, where L is a bifurcation parameter measuring the length of the system. To prepare the ground for the numerical scheme, we first rescale evolution equations (33) and (34) onto the canonical spatial domain $[-\pi,\pi]$ by making the transformations

$$z=\frac{L}{\pi}\hat{z},\quad t=\left(\frac{L}{\pi}\right)^2\hat{t},\quad H=\frac{\pi}{L}\hat{H},\quad \tilde{\Gamma}=\frac{\pi}{L}\hat{\Gamma}, \tag{43}$$

and defining the new domain parameter $\nu=\pi^2/L^2$. The transformed equations are

$$\hat{H}_t+\hat{H}\hat{H}_{\hat{z}}+\mathrm{i}\Lambda\nu^{-1}\sum_{n=-\infty}^{\infty}N(n\sqrt{\nu})\tilde{H}_n\mathrm{e}^{\mathrm{i}n\hat{z}}+\nu\hat{H}_{\hat{z}\hat{z}\hat{z}\hat{z}}-\hat{\Gamma}_{\hat{z}\hat{z}}=0, \tag{44}$$

where

$$\tilde{H}_n=\frac{1}{2\pi}\int_{-\pi}^{\pi}\hat{H}(\xi,t)\mathrm{e}^{-\mathrm{i}n\xi}\mathrm{d}\xi \tag{45}$$

are the coefficients in the Fourier expansion of H on the domain $[-\pi,\pi]$. Rescaled localized equation (37) is

$$\hat{H}_t+\hat{H}\hat{H}_{\hat{z}}+\nu\hat{H}_{\hat{z}\hat{z}\hat{z}\hat{z}}+2\Lambda\left(\frac{1}{\sqrt{\nu}}\hat{H}_{\hat{z}}-\frac{1}{15}\sqrt{\nu}\hat{H}_{\hat{z}\hat{z}\hat{z}}\right)-\hat{\Gamma}_{\hat{z}\hat{z}}=0. \tag{46}$$

The surfactant transport equation becomes

$$\hat{\Gamma}_t+(\hat{H}\hat{\Gamma})_{\hat{z}}=\eta\hat{\Gamma}_{\hat{z}\hat{z}}. \tag{47}$$

The equations are solved numerically using a pseudospectral method. We take the Fourier transform of Eq. (44) or Eqs. (46) and (47) and solve the resulting ODEs in Fourier space using the exponential time differencing scheme with Runge–Kutta ETD2RK of Cox and Matthews[25] (see Kassam and Trefethen,[26] for similar example calculations for PDEs). The scheme is spectral in space and second-order accurate in time. On implementing the scheme, the spatial domain $[-\pi,\pi]$ is discretized using M equally spaced points and the solution is advanced in time using a time step δt. Unless otherwise stated, all results to be presented in this paper were computed taking $M=128$ and $\delta t=5\times10^{-3}$.

Considering first solutions when there is no coupling between the film and the upper layer, $\Lambda=0$, we perform calculations starting from the initial condition,

$$\hat{H}(\hat{z},0)=0.1\nu^{-1/2}\sin n\hat{z},\quad \hat{\Gamma}(\hat{z},0)=\tilde{\Gamma}_0\nu^{-1/2}, \tag{48}$$

for integer n. Keeping in mind transformation (43), we observe that by adopting initial conditions (48) for a series of simulations performed for different ν and for fixed values of all of the other parameters, we are effectively following the evolution of perturbations with the same physical amplitude to a film with the same base surfactant concentration over computational domains of different lengths. First we examine the case $\nu=0.1$, $\Lambda=0$, $\tilde{\Gamma}_0=1.0$, and $\eta=1.0$. A perturbation of wavelength $2\pi/n$ on the canonical domain $[-\pi,\pi]$ corresponds to a perturbation of wavenumber $k=n\sqrt{\nu}$ in the physical domain. The linear stability analysis presented in Sec. III A reveals that, in the present case, the flow is linearly unstable if $n\sqrt{\nu}<0.79$ [see Fig. 2(a)]. We take $n=1$, in which case the flow is therefore linearly unstable since $\sqrt{\nu}=0.32$. In Fig. 3(a) we plot the energy signal $E(\hat{t})$ against time, where

$$E(\hat{t})\equiv\int_{-\pi}^{\pi}\hat{H}^2(\hat{z},\hat{t})\mathrm{d}\hat{z}. \tag{49}$$

As time increases, the energy signal approaches a plateau via a stretch of decaying oscillations, and the interfacial and surfactant waves saturate to the steady state traveling-wave profiles shown in Fig. 3(b). On increasing the diffusivity up to $\eta=2.0$, while keeping the other parameters the same, we find that the energy signal approaches a plateau monotonically and the saturated wave profiles are rather similar to those shown in Fig. 3(b). Increasing the diffusivity further and beyond a critical value produces a stable flow in accord with

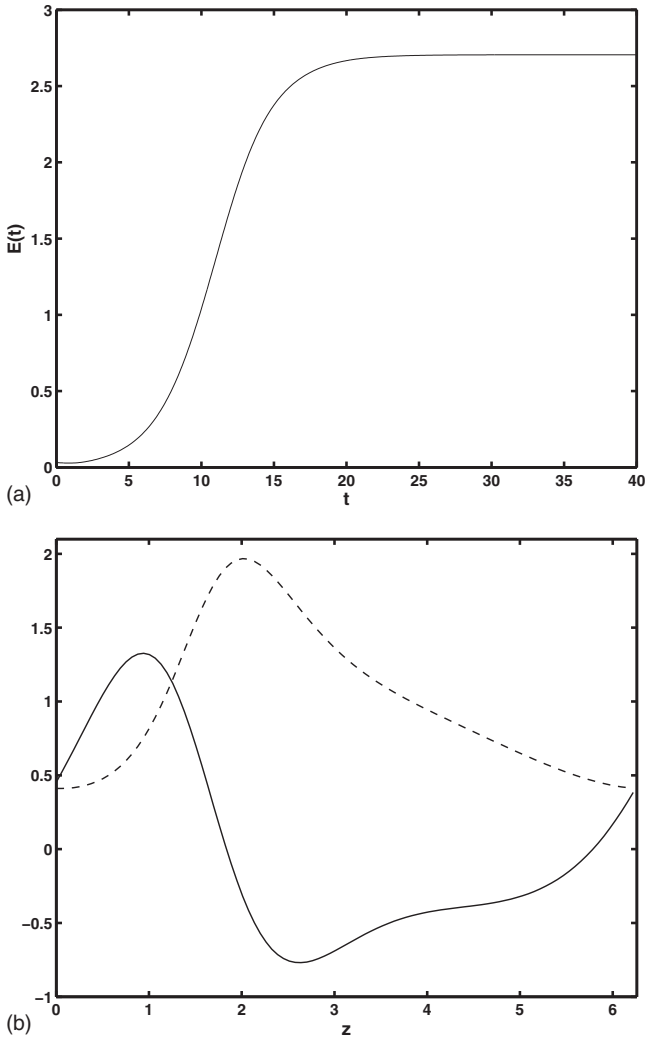

FIG. 3. Uncoupled flow with $\Lambda=0$, $\nu=0.1$, $\tilde{\Gamma}_0=1.0$, and $\eta=1.0$. (a) The energy signal $E(t)$ plotted against time and (b) the saturated wave profiles for $\hat{H}$ (solid line) and $\hat{\Gamma}(\hat{t})$ (dashed line) shown at $t=40.0$.

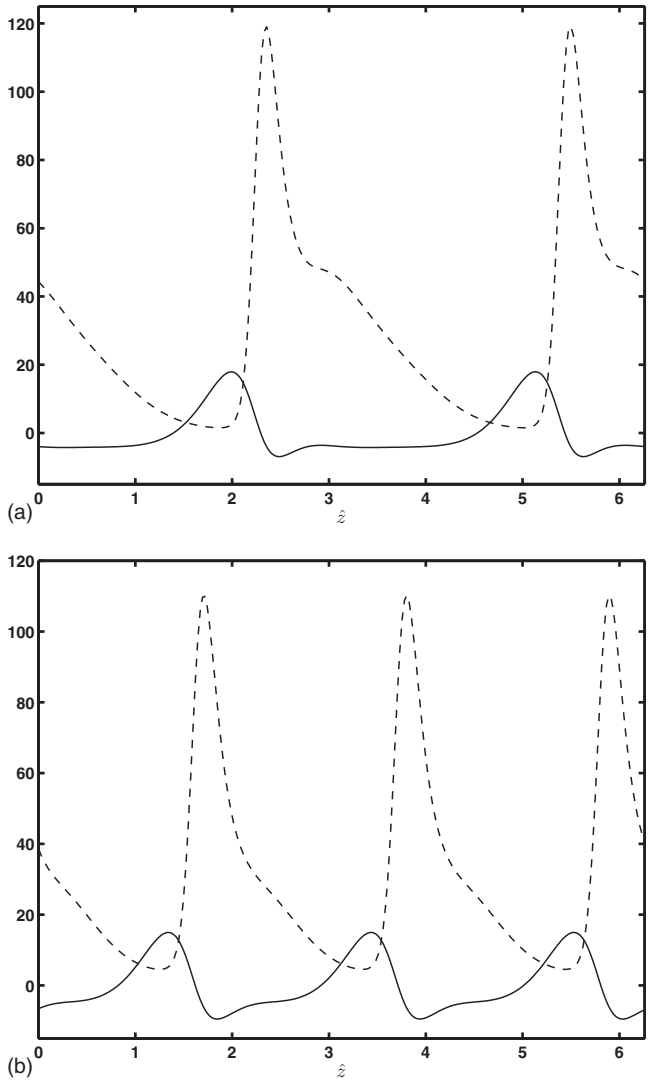

FIG. 4. Uncoupled flow with $\Lambda=0$, $\nu=0.1$, $\tilde{\Gamma}_0=10.0$, and $\eta=1.0$. The saturated wave profiles of $\hat{H}$ (solid lines) and $\hat{\Gamma}$ (broken lines) for initial condition (48) with (a) $n=1$ and (b) $n=3$. In both (a) and (b) the profiles are shown at $\hat{t}=10.0$.

the results of Sec. III A. Instead, increasing the base surfactant level beyond the value in Fig. 3, we find that modes with higher frequency n become linearly unstable according to the analysis in Sec. III A. Figure 4 displays saturated profiles for the case $\Lambda=0$, $\tilde{\Gamma}_0=10.0$, $\nu=0.1$, and $\eta=1.0$. The initial condition was taken to be Eq. (48) with $n=1$ and $n=3$ in Figs. 4(a) and 4(b), respectively. The initial perturbations, with $n=1$ and $n=3$, are both linearly unstable, and as can be seen lead to ultimately different saturated wave profiles.

As mentioned in Sec. I, it is possible that saturation such as that identified in Fig. 2(a) vanishes on reducing the value of ν. Lowering ν has the effect of widening the physical domain of computation, thereby admitting a larger number of linearly unstable modes. According to transformation (43) a wave of wavelength $2\pi/n$, for integer n, in the computational domain $[-\pi,\pi]$ has wavelength $2\pi/(n\sqrt{\nu})$ in the physical domain. To investigate the effect of extending the computational domain size, we lower ν and increase n so that $n^2\nu$ remains fixed and the physical wavelength of the computed wave does not change. In Fig. 5 we show the physical saturated wave profiles $\tilde{H}$ and $\tilde{\Gamma}$ resulting from a set of calculations performed for uncoupled flow with $\Lambda=0$, $\tilde{\Gamma}_0=1$, $\eta=1.0$ subject to initial conditions (48) for the sequence of values $\nu=(0.05)/4^m$, $n=2^m$ for $m=0,1,2,3$, so that $n^2\nu$ is fixed at 0.05. According to the analysis in Sec. III A, the flow is linearly unstable to modes in the physical domain with frequency n, such that $n\sqrt{\nu}<0.79$, so the initial perturbations for $m=0,1,2,3$ are all linearly unstable. The individual curves in the figure are virtually indistinguishable confirming that the same saturated solution is computed even as the physical domain size is repeatedly doubled.

We have also confirmed that saturated solutions are computed for increasingly small values of ν on taking a "white-noise" initial condition consisting of a random mixture of Fourier modes. We performed calculations for the same parameter values as in Fig. 3, namely, $\tilde{\Gamma}=1.0$, $\eta=1.0$, and $\Lambda=0.0$, but for smaller values of ν and subject to the initial condition

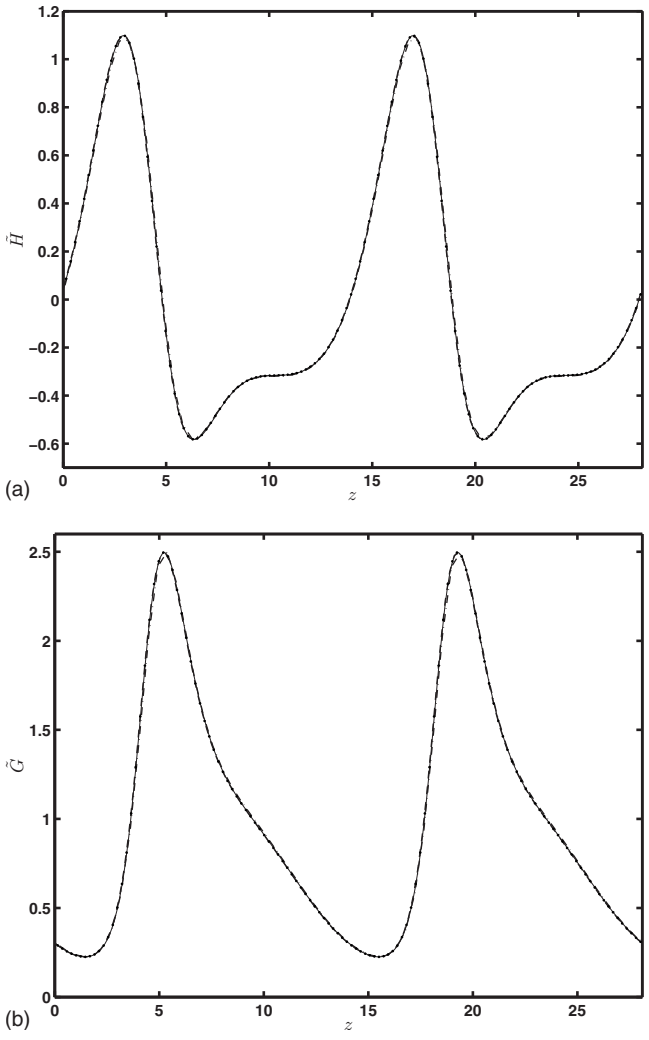

FIG. 5. Saturated wave profiles $\tilde{H}(z)$ and $\tilde{\Gamma}(z)$ for initial condition (48) for $\Lambda=0$, $\tilde{\Gamma}_0=1.0$, and $\eta=1.0$, with $(n,\nu)=(1,0.05)$ (solid line), $(n,\nu)=(2,0.0125)$ (dashed line), $(n,\nu)=(4,0.003\,125)$ (dot-dashed line), $(n,\nu)=(8,0.000\,781\,25)$ (dotted line). The solution for $n=8$ was computed by taking $M=1024$ and $\delta\hat{t}=5\times10^{-5}$.

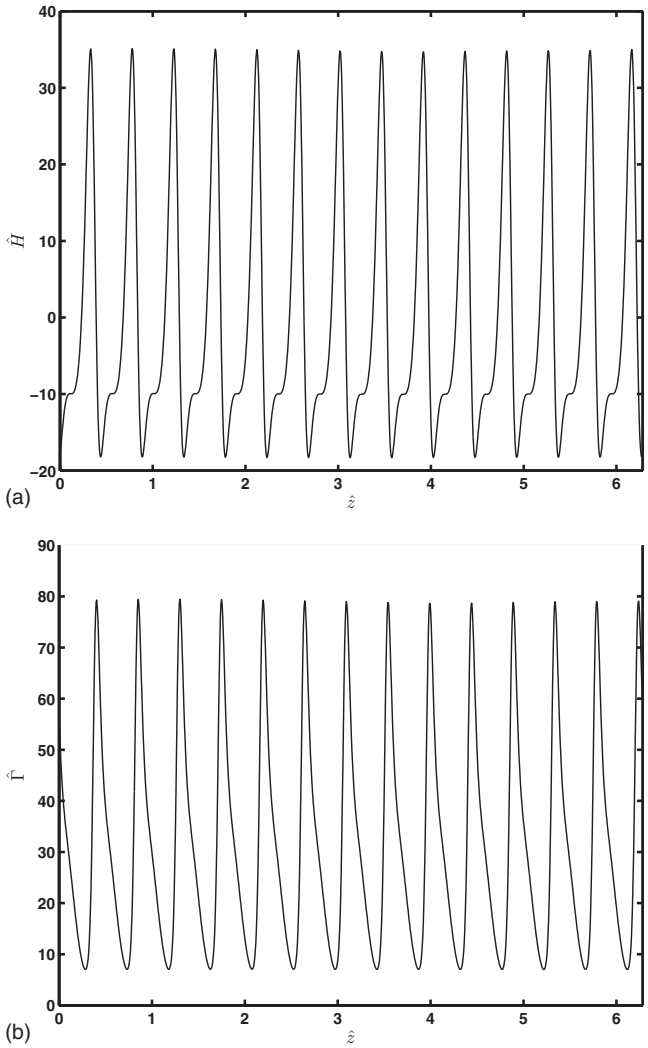

FIG. 6. Saturated wave profiles for uncoupled flow with $\Lambda=0$, $\nu=0.001$, $\tilde{\Gamma}_0=1.0$, and $\eta=1.0$ and $N=20$ Fourier modes in initial condition (50). (a) $\hat{H}$ and (b) $\hat{\Gamma}$. In both (a) and (b) the profiles are shown at $\hat{t}=6.0$.

$$\hat{H}(\hat{z},0)=0.1\nu^{-1/2}\sum_{n=0}^{N}h_n\sin n\hat{z},\quad \hat{\Gamma}(\hat{z},0)=\tilde{\Gamma}_0\nu^{-1/2},\qquad (50)$$

for some integer N, where the $0\le h_n\le 1$ are random numbers drawn from a uniform distribution. We carried out numerical simulations for $\nu=0.1$, 0.01, and 0.001. In each case, initial profiles (50) evolve toward fixed-form traveling-wave solutions. The saturated wave profiles for the case $\nu=0.001$ are shown in Fig. 6. These were computed using $\delta\hat{t}=10^{-5}$ and $M=1024$.

Next we study an example of coupled flow and set $\Lambda=0.5$, $\nu=0.1$, and $\eta=1.0$. According to the analysis in Sec. III A, for these parameter values a perturbation on the canonical domain $[-\pi,\pi]$ of wavelength 2π is linearly unstable when $\hat{\Gamma}_0>3.22$. In Fig. 7(a) we show the result of a calculation for $\hat{\Gamma}=3.5$ using initial condition (48). After an initial transient, the energy $E(\hat{t})$ rises monotonically and reaches a plateau at $\hat{t}\approx80$ by which time the film thickness and surfactant concentration profiles have settled into the fixed-form traveling-waves shown in the figure. For a larger base surfactant concentration, the rise of the energy during the simulation is nonmonotonic and $E(\hat{t})$ tends to a constant in an oscillatory manner similar to that shown in Fig. 3(a). For a sufficiently large value of $\tilde{\Gamma}_0$, the oscillations in the energy signal do not decay and $E(\hat{t})$ locks onto a periodic orbit. An example of this behavior is provided in Fig. 7(b) for the case $\tilde{\Gamma}_0=4.0$. The energy signal is displayed once it has settled into a periodic cycle after a long period of evolution. The corresponding long-term film thickness and surfactant concentration profiles are periodic traveling-waves, namely, waves which change their shape periodically within their traveling-wave frame. The period of the cycle shown in Fig. 7(b) is 8.41. Snapshots of the film thickness and surfactant concentration profiles, $\hat{H}$ and $\hat{\Gamma}$, respectively, taken at four time instants in one time cycle are displayed in Fig. 8.

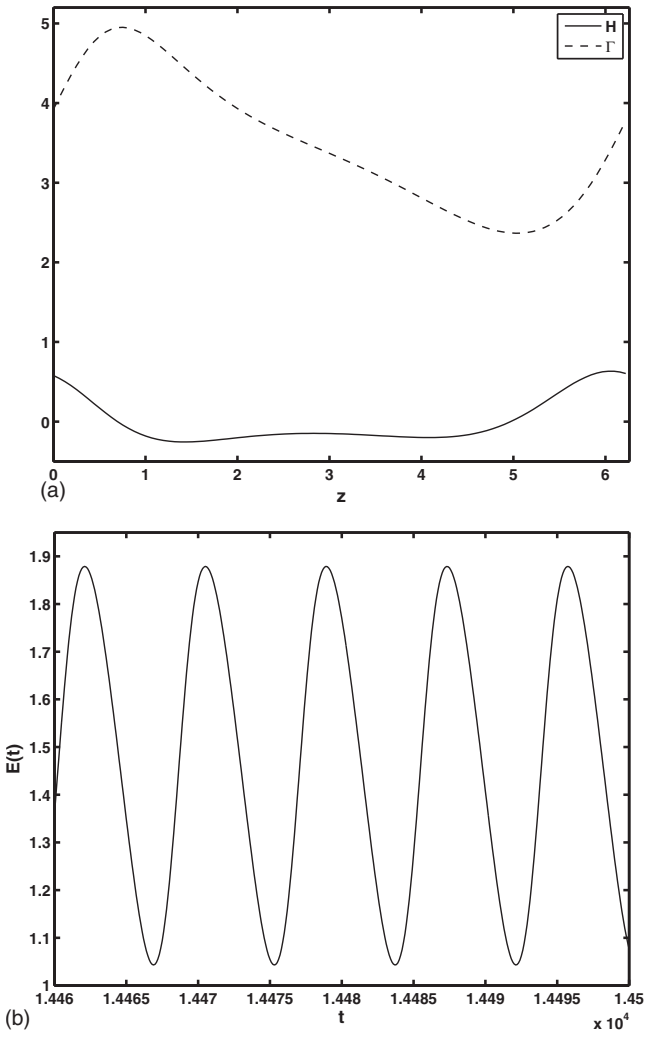

FIG. 7. The case $\Lambda=0.5$, $\nu=0.1$, and $\eta=1.0$. (a) The saturated profiles for $\hat{\Gamma}_0=3.5$ ($\tilde{\Gamma}_0=1.107$). $\hat{H}(\hat{t})$ and $\hat{\Gamma}(\hat{t})$ are shown as solid and broken lines, respectively. (b) The energy $E(\hat{t})$ shown against time when $\hat{\Gamma}_0=4.0$ ($\tilde{\Gamma}_0=1.265$).

IV. FINITE REYNOLDS NUMBER FLOW IN THE UPPER LAYER: $R_2=O(1)$

In this section, we assume that the Reynolds numbers in the upper layer and the film are both of order unity. In this case, same scalings (13) apply, but the film expansions are now written as

$$u_1=\bar{u}_1(y)+\epsilon^3\hat{U}_1(x,\zeta,t)+\cdots,\quad v_1=\epsilon^4\hat{V}_1(x,\zeta,t)+\cdots, \tag{51a}$$

$$p_1=\bar{p}_1+\epsilon\hat{P}_1(x,\zeta,t)+\cdots, \tag{51b}$$

where $\zeta=y/\epsilon$, and the expansions in the upper layer are written as

$$u_2=\bar{u}_2(y)+\epsilon^2\hat{U}_2(x,y,t)+\cdots,\quad v_2=\epsilon^2\hat{V}_2(x,y,t)+\cdots, \tag{52a}$$

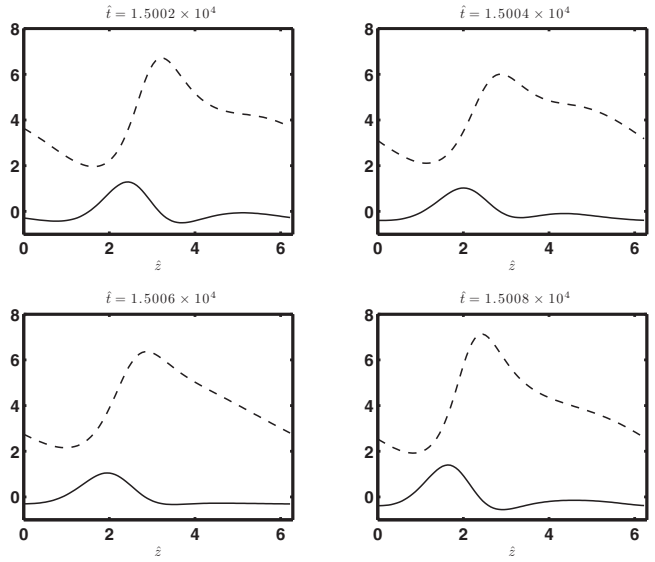

FIG. 8. Profiles for the case shown in Fig. 7(b) for equally spaced times during one period, which is of duration 8.41 time $\hat{t}$ units. The film thickness profiles, $\hat{H}$, and the surfactant concentration profiles, $\hat{\Gamma}$, are shown as solid and broken lines, respectively.

$$p_2=\bar{p}_2+\epsilon^2\hat{P}_2(x,y,t)+\cdots. \tag{52b}$$

At leading order, the normal and tangential stress balances are identical to Eqs. (19) and (20), respectively, but with hat superscripts placed over the variables and with λ replaced by R_2 in Eq. (19). The solution in the film proceeds as in Sec. III, despite slightly different expansions (51), and once again we derive the equation for H given in Eq. (24). As before, the right-hand side is determined by the solution in the upper layer.

In the upper layer, substituting expansions (52) into Eq. (1) and retaining terms at leading order, we obtain the linearized Navier–Stokes equations,

$$\bar{U}U_{2x}+\bar{U}'V_2=-P_{2x}+\frac{1}{R_2}(U_{2xx}+U_{2yy}), \tag{53a}$$

$$\bar{U}V_{2x}=-P_{2y}+\frac{1}{R_2}(V_{2xx}+V_{2yy}), \tag{53b}$$

$$U_{2x}+V_{2y}=0, \tag{53c}$$

where $\bar{U}=-a_2y^2+(1+a_2)y$ and a prime denotes differentiation with respect to y. Next, we introduce the streamfunction $\hat{\psi}$ defined so that $\hat{U}_2=\hat{\psi}_y$ and $\hat{V}_2=-\hat{\psi}_x$, and take the Fourier transform of Eq. (53a). Eliminating the pressure we find

$$\mathrm{i}kR_2[\bar{U}(\hat{\psi}^*_{yy}-k^2\hat{\psi}^*)+2a_2\hat{\psi}^*]=\hat{\psi}^*_{yyyy}-2k^2\hat{\psi}^*_{yy}+k^4\hat{\psi}^*. \tag{54}$$

The boundary conditions are Eqs. (28) and (29) with hat superscripts placed over the streamfunctions. Writing $\hat{\psi}^*=(1/m)(1-m)(a_1+m)H^*F(y)$, we find that F satisfies the system

$$F^{(iv)} - [2k^2 + ikR_2\bar{U}]F'' + [ik^3R_2\bar{U} - 2ikR_2a_2 + k^4]F = 0, \tag{55a}$$

$$F(0) = 0, \quad F'(0) = 1, \quad F(1) = F'(1) = 0, \tag{55b}$$

which we may solve numerically using MATLAB, for example. Referring to Eq. (21) in Sec. III, in the present case we have $T|_{y=0} = (\hat{U}_{2xy} + \hat{V}_{2xx})_{y=0}$, and in Fourier space $T^*|_{y=0} = ik\hat{\psi}^*_{yy}$. Accordingly we derive a canonical evolution equation identical to Eq. (33) but with Eq. (31) replaced by

$$N(k) = -(k/2)F''(0), \tag{56}$$

where the right-hand side is found by solving system (55).

To obtain the localized form of the evolution equation, it is a straightforward calculation to obtain a series solution to Eq. (55) for small k in the form

$$F(y) = F_0(y) + kF_1(y) + k^2F_2(y) + \cdots. \tag{57}$$

We find that $F_0 = y - 2y^2 + y^3$ together with increasingly lengthy polynomial expressions for the higher order terms. In particular, we have

$$F''(0) = -4 - \frac{1}{30}\left(1 + \frac{a_2}{7}\right)iR_2k - \left(\frac{4}{15} + \frac{1}{210}\left[\frac{1}{20} + \frac{a_2}{90} + \frac{a_2^2}{693}\right]R_2^2\right)k^2 + O(k^3). \tag{58}$$

Disregarding terms of $O(k^3)$ in Eq. (58) and substituting into Eq. (56), we obtain the localized evolution equation for the film thickness,

$$H_\tau + HH_z + H_{zzzz} - \tilde{\Gamma}_{zz} + 2\Lambda(H_z + \hat{\alpha}R_2H_{zz} - \hat{\beta}H_{zzz}) = 0, \tag{59}$$

where

$$\hat{\alpha} = \frac{1}{120}\left(1 + \frac{a_2}{7}\right), \quad \hat{\beta} = \frac{1}{15} + \frac{1}{840}\left[\frac{1}{20} + \frac{a_2}{90} + \frac{a_2^2}{693}\right]R_2^2, \tag{60}$$

and Λ is given in Eq. (35). The surfactant transport equation is given by Eq. (47).

A. Linear stability analysis

We follow the same procedure as in Sec. III A and perturb about the base flow as in Eq. (38). The dispersion relation for the complex growth rate is Eq. (39) with $N(k) = -F''(0)/2$, where $F''(0)$ is given by Eq. (58). We find the small k expansions for the growth rates,

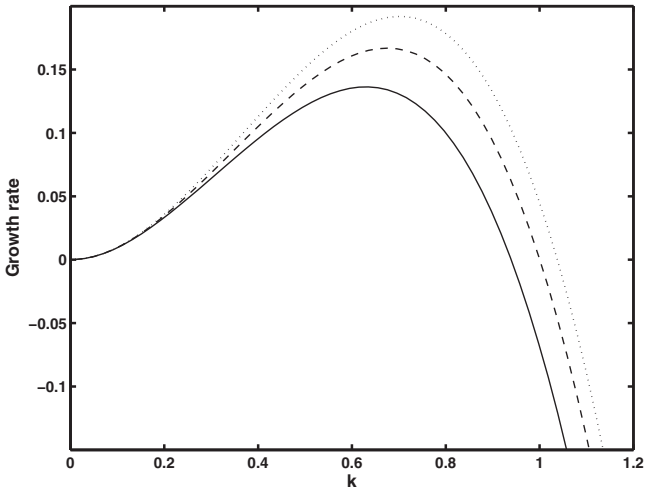

FIG. 9. Dominant growth rate for the case $\Lambda = 0.5$, $\tilde{\Gamma}_0 = 2.0$, $\eta = 1$, $a_2 = 0$, and $R_2 = 0$ (solid line), $R_2 = 25$ (dashed line), and $R_2 = 50$ (dotted line).

$$s_1 = \frac{(\tilde{\Gamma}_0 - 2\eta\Lambda)}{2\Lambda}k^2 + \cdots,$$
$$s_2 = \frac{[R_2\Lambda^2(7 + a_2) - 210\tilde{\Gamma}_0]}{420\Lambda}k^2 + \cdots, \tag{61}$$

and it is found that both s_1 and s_2 are negative for large k. When $\Lambda > 0$ and the film is more viscous than the upper layer, small k expansions (61) suggest that instability will occur for long waves if either of the following two conditions hold:

$$\tilde{\Gamma}_0 > 2\eta\Lambda, \quad \tilde{\Gamma}_0 < \tfrac{1}{210}(7 + a_2)R_2\Lambda^2. \tag{62}$$

The first condition is the same as that identified for Stokes flow in Sec. III. When $\Lambda < 0$ so that the upper layer is more viscous than the film, the condition for long-wave instability is simply

$$\tilde{\Gamma}_0 > \tfrac{1}{210}(7 + a_2)R_2\Lambda^2. \tag{63}$$

In Fig. 9 we display the growth rates as a function of wavenumber for the three different Reynolds numbers $R_2 = 0$, =25, and $R_2 = 50$ when $a_2 = 0$, $\Lambda = 0.5$, $\tilde{\Gamma} = 1.0$, and $\eta = 1.0$. The cutoff wavenumbers are $k = 0.94$, 1.00, and 1.04 for $R_2 = 0$, 25, and 50, respectively. The second stability criterion in Eq. (62) confirms that inertia is able to destabilize a flow which is stable at zero Reynolds number, as predicted by Yih[1] for a clean interface. When surfactant is not present and the lower layer is more viscous than the upper layer, corresponding to $\Lambda > 0$, the second condition in Eq. (62) indicates that the flow is unstable when $R_2 > 0$ in agreement with the observation of Hooper;[3] conversely, when $\Lambda < 0$ and the upper layer is more viscous than the lower layer, condition (63) shows that the flow is stable. Furthermore, it is interesting to note that according to Eq. (62), it is possible to have a stable flow with both inertia and surfactant present, provided that $2\eta\Lambda > (7 + a_2)R_2\Lambda^2/210$.

B. Weakly nonlinear calculations

The localized equation for film thickness (59) has the same basic form as that derived by Kas-Danouche *et al.*[16] for core-annular flow with a thin outer layer and with Stokes flow in the upper layer. In that axisymmetric problem, the H_{zz} term appearing in the equation arises from the azimuthal curvature contribution. In the present case, the H_{zz} term has arisen due to the inclusion of inertia in the upper layer flow. The H_{zzzz} term in Eq. (59) stabilizes short waves while the H_{zz} term destabilizes long waves if Λ is positive and stabilizes them otherwise. At the same time, the nonlinear term in Eq. (59) channels energy from long waves to short waves. This feedback of energy from waves being stabilized to those being destabilized raises the possibility of a richer set of dynamics than that encountered in Sec. III. For example, Kas-Danouche *et al.*[16] computed a host of different phenomena including traveling-waves, periodic traveling-waves, and chaotic attractors.

We computed solutions of weakly nonlinear equations (59) and (47) rescaled onto the canonical domain $[-\pi,\pi]$ via transformation (43) using the pseudospectral method described in Sec. III B and subject to initial conditions (48) with $n=1$. This means that as ν is varied, with all other parameters held fixed, we are effectively considering the same physical film thickness and the same base surfactant concentration level, but over different length computational domains. Preliminary numerical experimentation indicated that solutions for the parameter values $R_2=25$, $a_2=0$, $\Lambda=0.5$, $\tilde{\Gamma}_0=2.0$, and $\eta=1.0$ cover the range of characteristic dynamical behavior for the system. Therefore, to illustrate the typical behavior of solutions to weakly nonlinear systems (59) and (47), we examine solutions for this parameter set in detail. According to the analysis in Sec. IV A, the flow is linearly unstable since the first of conditions (62) is satisfied for these parameter values. Referring to the dashed line in Fig. 9, a perturbation corresponding to initial condition (48) will grow in amplitude provided that $\sqrt{\nu}<1.00$. In Tables I and II we summarize the results of an extensive series of calculations carried out for different values of the domain length parameter ν. Table I shows the types of flow solution obtained for a range of values of ν between 0.01 and 1.1.

A key to the shorthand for the flow types is included in the caption. For $\nu=1.1$ the flow is stable, the initial perturbation decays and the system returns to the basic state with a uniform film thickness. To help in characterizing the dynamical behavior for a general value of ν, we constructed return maps of the solutions by plotting on a graph the points (m_i,m_{i+1}), where m_i is the ith maximum of the signal $E(\hat{t})$. If the return map contains just one point, the flow is time-periodic with one distinct maximum in the $E(\hat{t})$ signal, corresponding to a periodic traveling-wave PTW[1] in the notation of Table I. If the return map contains two points, the flow is time-periodic with two distinct maxima in the $E(\hat{t})$ signal, corresponding to a periodic traveling-wave PTW[2]. Quasiperiodic solutions are indicated in the return maps by continuous-looking curves, which are densely populated with points. Chaotic dynamics are suggested by intricate structures in the return maps that include folds and self-similarity.

TABLE I. Flow characteristics for solutions to Eqs. (59) and (47) subject to Eq. (48) with $n=1$ for $R_2=25$, $a_2=0$, $\Lambda=0.5$, $\tilde{\Gamma}_0=2.0$, and $\eta=1.0$. ST: stable flow, TW: traveling-wave, PTW[m]: periodic traveling-wave with m maxima in each time period, QP: quasiperiodic, and C: chaotic.

ν	Flow type
1.1	ST
0.9	TW
0.8	TW
0.7	TW
0.6	TW
0.5	TW
0.4	TW
0.3	TW
0.2	TW
0.1	TW
0.09	TW
0.08	PTW[1]
0.07	PTW[1]
0.06	TW
0.05	TW
0.04	PTW[1]
0.03	PTW[2]
0.02	PTW[1]
0.01	C

Traveling-wave solutions become apparent after only very short computational run times. For example, when $\nu=0.1$, a simulation with $M=256$ and $\delta\hat{t}=10^{-4}$ locks on to the traveling-wave solution at $\hat{t}\approx 10$. Very long run times are required to elucidate the more intricate structures in the return maps. Calculations for the chaotic and quasiperiodic solutions were performed using MATLAB with $M=256$ and $\delta\hat{t}=10^{-5}$ and, for the longest simulations, required considerable CPU time (on the order of days) on a Mac Pro Desktop computer with a 3GHz Intel processor.

TABLE II. See the caption for Table I.

ν	Flow type
0.068 75	PTW[1]
0.067 187 5	PTW[2]
0.065 625	PTW[3]
0.064 062 5	PTW[2]
0.062 5	TW
0.019	PTW[1]
0.018	TW
0.017	TW
0.016	TW
0.015	QP
0.014	QP
0.013	QP
0.012 75	C
0.012 5	PTW[1]
0.012	C

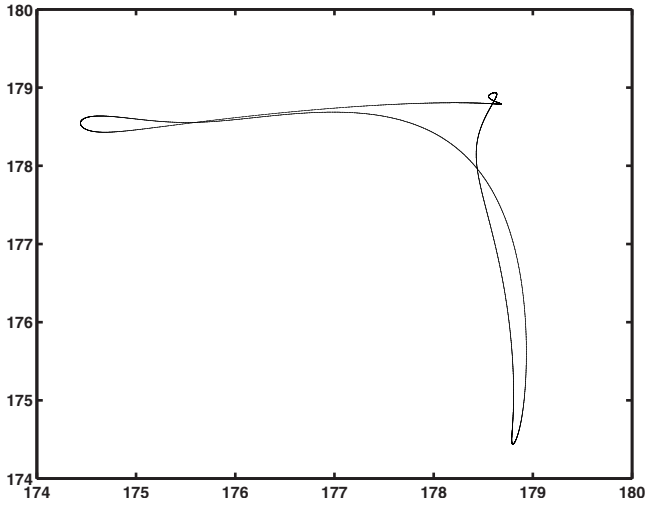

FIG. 10. Return map of the maxima of the energy signal for $\nu=0.014$ when $R_2=25$, $a_2=0$, $\Lambda=0.5$, $\tilde{\Gamma}_0=2.0$, and $\eta=1$.

From the results shown in Table I it appears that for $0.1 \leq \nu \leq 1.00$, the film thickness profile settles down to a traveling-wave. More complex behavior for $\nu < 0.1$ is suggested by the appearance of periodic traveling-wave solutions and chaos. More detailed investigation of the solution characteristics for these smaller values of ν are provided in Table II. The return map of the maxima of $E(\hat{t})$ for the quasiperiodic solution at $\nu=0.014$ is displayed in Fig. 10. The map forms a closed loop of densely packed individual points. The maxima of $E(\hat{t})$ and the return map of the maxima for the solution when $\nu=0.012$ are shown in Fig. 11. The chaotic nature of the solution is suggested by the intricate structures in the return map. Finer structure is found by zooming in on the individual strands seen in the figure to reveal foldings and self-similarity which are the hallmarks of chaotic dynamics (e.g., Ref. 27).

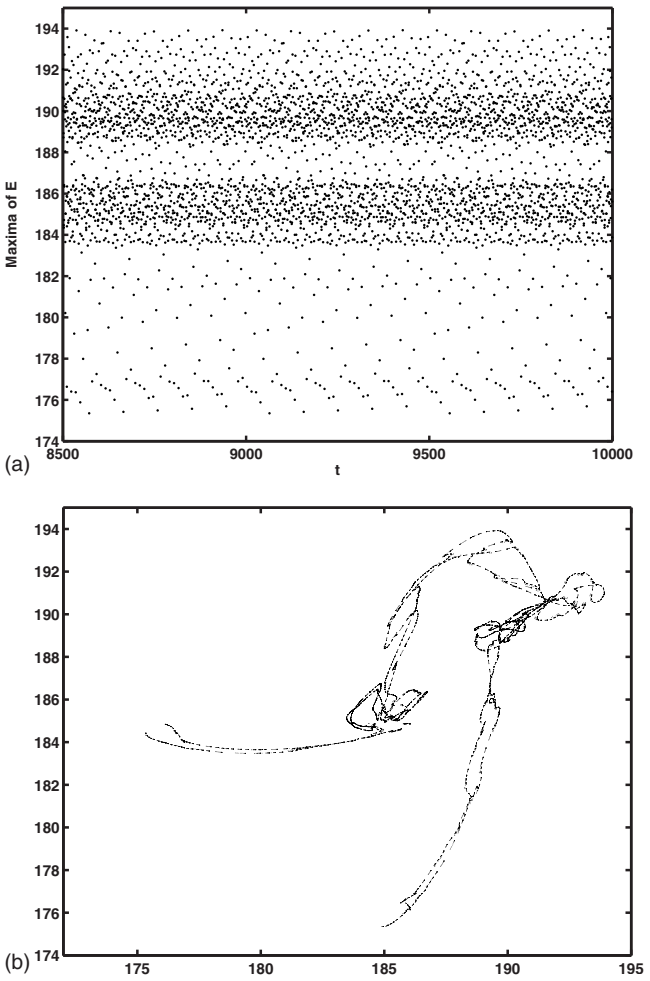

FIG. 11. Chaotic dynamics for $\nu=0.012$ when $R_2=25$, $a_2=0$, $\Lambda=0.5$, $\tilde{\Gamma}_0=2.0$, and $\eta=1$. (a) Maxima of the energy signal $E(\hat{t})$ and (b) return map of the maxima.

V. DISCUSSION

We have demonstrated that the weakly nonlinear approach devised by Papageorgiou *et al.*[15] for core-annular flow in the thin annulus limit, and later developed by Kas-Danouche *et al.*[16] to include the effect of an insoluble surfactant, may be applied to the problem of two-layer channel flow. Working on the assumption of a thin lower layer in comparison to the thickness of the overlying fluid, we derived a pair of weakly nonlinear equations describing the evolution of the thin film thickness and the concentration of surfactant. The film dynamics are coupled to the dynamics in the thicker layer through a nonlocal integral term. When the Reynolds number is asymptotically small and on the order of the film thickness, the dynamics in the thicker layer are controlled by the linear equations of Stokes flow. We performed a linear stability analysis and proved that when the film is less viscous than the overlying fluid, the flow is unstable if the base surfactant concentration level exceeds a threshold value. When the film is more viscous than the overlying fluid, the flow is linearly unstable for any nonzero value of the base surfactant concentration. The weakly nonlinear evolution equation for the film thickness H differs from that derived by Kas-Danouche *et al.*[16] for the axisymmetric problem at asymptotically small Reynolds number in that the destabilizing term proportional to H_{zz} is absent in the channel equation. As a consequence, the film dynamics are considerably simpler in the latter case. Our numerical simulations revealed the existence of saturated traveling-wave solutions.

When the Reynolds number is of order unity, the flow in the thicker fluid layer is governed by the linearized Navier–Stokes equations. A linear stability analysis showed that the film is unstable if the base surfactant concentration either exceeds the same threshold as found previously for Stokes flow in the upper layer, or else lies below a critical value dependent on the Reynolds number. The weakly nonlinear equation for the film thickness includes a term proportional to $R_2 H_{zz}$ suggesting a richer set of possible dynamical behavior than that found in the Stokes flow case. A case study carried out on one representative set of parameter values found the existence of traveling-waves, periodic traveling-waves, and quasiperiodic and chaotic solutions.

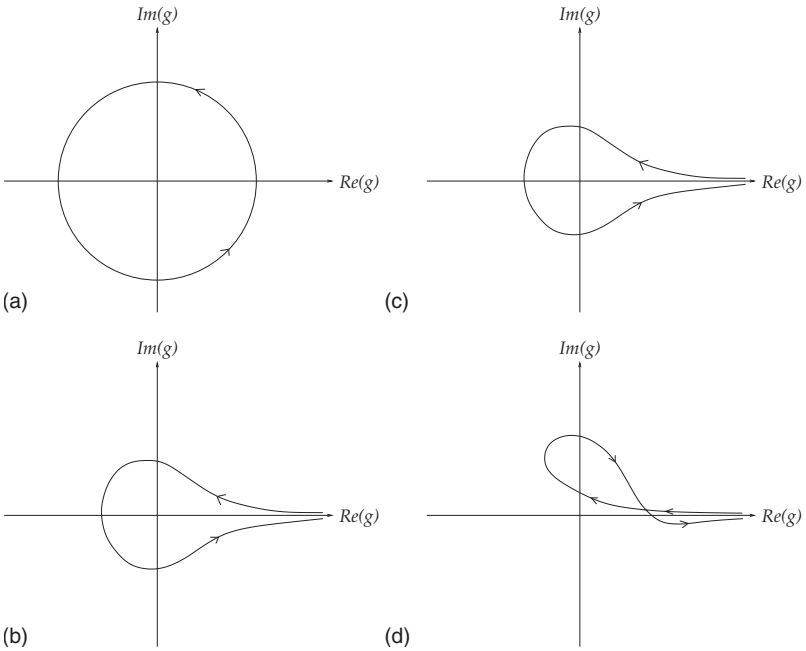

FIG. 12. Sketches of the images of sections of the contour C in the complex g plane. The image of the semicircular arc is shown in (a). The image of the straight segment is shown in the remaining panels for (b) $c_i>0$, (c) $c_i<0$ and $c_i+b_r\beta<0$, and (d) $c_i<0$ and $c_i+b_r\beta>0$. The arrows indicate the direction of travel as we move anticlockwise around the semicircular contour C. For (b)–(d) the sketches show only the qualitative behavior of the image contours.

ACKNOWLEDGMENTS

D.T.P. was supported in part by the National Science Foundation Grant No. DMS-0707339. The authors would like to thank the referees for very helpful comments and suggestions.

APPENDIX: PROOF OF LINEAR STABILITY

With reference to the linear stability analysis presented in Sec. III A, we establish that small perturbations are linearly unstable if and only if $\tilde{\Gamma}_0>2\eta\Lambda$ when $\Lambda>0$. We begin by writing dispersion relation (39) in the form

$$f(z)\equiv z^2+b(k)z+c(k)=0, \tag{A1}$$

where $b=b_r+\mathrm{i}b_i$ and $c=c_r+\mathrm{i}c_i$ are complex functions of k with real and imaginary parts given by

$$b_r=k^4+\eta k^2, \quad b_i=\Lambda N(k),$$
$$c_r=\eta k^6, \quad c_i=\eta\Lambda k^2N(k)-k^3\tilde{\Gamma}_0, \tag{A2}$$

with $N(k)$ given by Eq. (31). Since $N(k)>0$ for $k>0$ and $\Lambda>0$, we have that

$$b_r(k)>0, \quad b_i(k)>0, \quad c_r(k)>0. \tag{A3}$$

Proceeding we consider a semicircular contour C of radius R with straight edge occupying $x=0$, $-R\le y\le R$ in the complex $z=x+\mathrm{i}y$ plane, where the arc of the semicircle resides in the left-hand plane, $x<0$. Invoking the argument principle (e.g., Ablowitz and Fokas[24]), we have

$$\frac{1}{2\pi\mathrm{i}}\int_C\frac{f'(z)}{f(z)}\mathrm{d}z=n-p=\frac{1}{2\pi}[\arg f(z)]_C, \tag{A4}$$

where n and p are, respectively, the number of zeros and poles of $f(z)$ inside C, and $(1/2\pi)[\arg f(z)]_C$, is the winding number of $f(z)$. Since $f(z)$ clearly does not have any poles inside C, we may set $p=0$. Following a standard methodology, we aim to determine n in the limit $R\to\infty$.

Writing $z=R\mathrm{e}^{\mathrm{i}\theta}$ on the curved part of C, we find that $f\sim g$ for large R, where $g\equiv R^2\mathrm{e}^{2\mathrm{i}\theta}$. Traversing the semicircular part of C in the anticlockwise direction corresponds to following the path circular image contour in the complex g plane in the directions of the arrows shown in Fig. 12(a). Since the image contour winds once around the origin, giving a winding number of 1 for the semicircular part of the contour. On the straight segment of C, where $z=\mathrm{i}y$, the complex function $f(z)$ may be expressed in the form $f=-g$, where

$$g\equiv(y-\alpha)(y-\beta)-\mathrm{i}(c_i+b_ry), \tag{A5}$$

and where the real numbers α and β are given by

$$\alpha=\tfrac{1}{2}(-b_i-\sqrt{b_i^2+4c_r}), \quad \beta=\tfrac{1}{2}(-b_i+\sqrt{b_i^2+4c_r}). \tag{A6}$$

From Eqs. (A3) and (A5) we see that $\alpha<-b_i<0$ and $\beta>0$. Consequently, since $b_r>0$ from Eq. (A3), we may establish that $c_i+b_r\alpha<c_i-b_rb_i$. Since $c_i-b_rb_i=-k^3\tilde{\Gamma}_0-k^4\Lambda N(k)<0$ from Eq. (A2), it follows that

$$c_i+b_r\alpha<0. \tag{A7}$$

According to Eq. (A5), the image of the straight segment of C in the complex g plane will cross the imaginary g axis when $y=\alpha$ and $y=\beta$ at the points $\mathrm{Im}(g)=-(c_i+b_r\alpha)$ and $\mathrm{Im}(g)=-(c_i+b_r\beta)$. The former value is always negative according to Eq. (A7), but the latter value may be either positive or negative. There are three subcases to consider.

(i) $c_i>0$. Since we have already established that $\beta>0$ and $b_r>0$, if $c_i>0$ we have that $c_i+b_r\beta>0$. Moving from $y=-\infty$ up to $y=\infty$ along the straight segment of C corresponds to following the image contour in the g

plane, which is sketched in Fig. 12(b), in the direction shown by the arrows. Since the image contour encircles the origin once, the winding number for the straight segment in this case is 1.

(ii) $c_i<0$ and $c_i+b_r\beta>0$. In this case we know that $c_i+b_r\alpha<0$. The image of the straight segment is sketched in Fig. 12(c). The image contour encircles the origin once, and so the winding number for the straight segment is 1.

(iii) $c_i<0$ and $c_i+b_r\beta<0$. As for case (ii) we know that $c_i+b_r\alpha<0$. The image of the straight segment is sketched in Fig. 12(d). Since the image contour does not encircle the origin, the winding number for the straight segment is zero.

In conclusion, in case (i) the total winding number for the contour C is 2, which implies that $n=2$. Accordingly, both of the zeros of $f(z)$ lie in the left-hand plane and the flow is linearly stable. In case (ii) the total winding number for C is 2, so that the flow is linearly stable. In case (iii) the total winding number for C is 1 and so $n=1$. One of the poles lies in the right-hand plane, and the flow is linearly unstable.

To investigate the conditions under which case (iii) obtains, we begin by noting that $N(k)>2k$ for $k>0$. To demonstrate this we consider the difference $N(k)-2k=kP(k)/Q(k)$, say, where $P(k)=k^2+k\cosh k\sinh k+2-2\cosh^2 k$ and $Q(k)=\cosh^2 k-1-k^2$. We have $Q'(k)=2(\sinh k\cosh k-k)>0$ for all k and so, since $Q(0)=0$, we have that Q is non-negative for all $k>0$. It, therefore, remains to show that P is also non-negative. Through straightforward calculation we find that $P(0)=P'(0)=P''(0)=P'''(0)=0$ and that $P^{(iv)}(k)=16k\sinh k\cosh k>0$. Hence P''' is an increasing function of k and so $P'''>0$ for $k>0$. Arguing along similar lines, we conclude that $P\geq 0$ for $k>0$ and hence $N(k)>2k$ for $k>0$. Following this, we may write

$$c_i(k)=k^2[\eta\Lambda N(k)-k\tilde{\Gamma}_0]>k^3(2\eta\Lambda-\tilde{\Gamma}_0). \tag{A8}$$

If $\tilde{\Gamma}_0<2\eta\Lambda$ then Eq. (A8) implies that $c_i>0$ for all $k>0$ and so the flow is linearly stable according to case (i) above. If $\tilde{\Gamma}_0>2\eta\Lambda$ then instability occurs for sufficiently small k. To see this, we first note that $c_i\sim c_i+b_r\beta\sim k^3(2\eta\Lambda-\tilde{\Gamma}_0)$ as $k\to 0$. Therefore, both $c_i<0$ and $c_i+b_r\beta<0$ for sufficiently small k, fulfilling the conditions of case (iii) above and guaranteeing linear instability.

[1] C. S. Yih, "Instability due to viscosity stratification," J. Fluid Mech. **27**, 337 (1967).
[2] A. P. Hooper and W. G. C. Boyd, "Shear-flow instability at the interface between two viscous fluids," J. Fluid Mech. **128**, 507 (1983).
[3] A. P. Hooper, "Long-wave instability at the interface between two viscous fluids: Thin-layer effects," Phys. Fluids **28**, 1613 (1985).
[4] A. P. Hooper and R. Grimshaw, "Nonlinear instability at the interface between two viscous fluids," Phys. Fluids **28**, 37 (1985).
[5] F. Charru and J. Fabre, "Long waves at the interface between two viscous fluids," Phys. Fluids **6**, 1223 (1994).
[6] A. L. Frenkel and D. Halpern, "Stokes flow instability due to interfacial surfactant," Phys. Fluids **14**, L45 (2002).
[7] D. Halpern and A. L. Frenkel, "Destabilization of a creeping flow by interfacial surfactant: linear theory extended to all wavenumbers," J. Fluid Mech. **485**, 191 (2003).
[8] M. G. Blyth and C. Pozrikidis, "Effect of surfactants on the stability of two-layer channel flow," J. Fluid Mech. **505**, 59 (2004).
[9] H.-H. Wei, "On the flow-induced Marangoni instability due to the presence of surfactant," J. Fluid Mech. **544**, 173 (2005).
[10] C. Pozrikidis, "Effect of inertia on the Marangoni instability of two-layer channel flow, Part I: numerical simulations," J. Eng. Math. **50**, 311 (2004).
[11] M. G. Blyth and C. Pozrikidis, "Effect of inertia on the Marangoni instability of the two-layer channel flow. Part II. Normal-mode analysis," J. Eng. Math. **50**, 329 (2004).
[12] A. L. Frenkel and D. Halpern, "Effect of inertia on the insoluble-surfactant instability of a shear flow," Phys. Rev. E **71**, 016302 (2005).
[13] A. L. Frenkel and D. Halpern, "Strongly nonlinear nature of interfacial-surfactant instability of Couette flow," Int. J. Pure Appl. Maths **29**, 205224 (2006) (as of July 2010, this article is available at arXiv:nlin/061025).
[14] D. Halpern and A. L. Frenkel, "Nonlinear evolution, travelling waves, and secondary instability of sheared-film flows with insoluble surfactants," J. Fluid Mech. **594**, 125 (2008).
[15] D. T. Papageorgiou, C. Maldarelli, and D. S. Rumschitzki, "Nonlinear interfacial stability of core-annular film flows," Phys. Fluids A **2**, 340 (1990).
[16] S. A. Kas-Danouche, D. T. Papageorgiou, and M. Siegel, "Nonlinear dynamics of core-annular flows in the presence of surfactant," J. Fluid Mech. **626**, 415 (2009).
[17] D. D. Joseph and Y. Y. Renardy, *Fundamentals of Two-Fluid Dynamics* (Springer-Verlag, Berlin, 1993).
[18] H. Wong, D. Rumschitzki, and C. Maldarelli, "On the surfactant mass balance at a deforming fluid interface," Phys. Fluids **8**, 3203 (1996).
[19] X. Li and C. Pozrikidis, "The effect of surfactants on drop deformation and on the rheology of dilute emulsions in Stokes flow," J. Fluid Mech. **341**, 165 (1997).
[20] S. Chandrasekhar, *Hydrodynamic and Hydromagnetic Stability* (Dover, New York, 1981).
[21] H.-H. Wei and D. Rumschitzki, "The effects of insoluble surfactants on the linear stability of a core-annular flow," J. Fluid Mech. **541**, 115 (2005).
[22] We are grateful to a referee who pointed out to us that our assumptions correspond to taking small C in Frenkel and Halpern's equations (11) and (12) (Ref. 13). To see this, write $h=1+\epsilon H$, $\tau=\epsilon^{1/2}t$, and $z=\epsilon^{-1/2}(x-t)$, and $C=\epsilon^{5/2}$ in equations (11) and (12) of Ref. 13 [or, equivalently, (2.14) and (2.15) in Ref. 14]. At leading order they reduce to Eqs. (33) and (34) with $\Lambda=0$ and $\eta=0$. Moreover, Ref. 13 contains some simulation results for the small value $C=10^{-2}$ which are similar to those shown in Fig. 5 here for the uncoupled case $\Lambda=0$.
[23] Y. S. Smyrlis and D. T. Papageorgiou, "The effects of generalized dispersion on dissipative dynamical systems," Appl. Math. Lett. **11**, 93 (1998).
[24] M. J. Ablowitz and A. S. Fokas, *Complex Variables: Introduction and Applications* (Cambridge University Press, Cambridge, 1997).
[25] S. M. Cox and P. C. Matthews, "Exponential time differencing for stiff systems," J. Comput. Phys. **176**, 430 (2002).
[26] A.-K. Kassam and L. N. Trefethen, "Fourth-order time-stepping for stiff PDEs," SIAM J. Sci. Comput. (USA) **26**, 1214 (2005).
[27] P. Bergé, Y. Pomeau, and C. Vidal, *Order Within Chaos-Towards a Deterministic Approach to Turbulence* (Wiley-Interscience, New York, 1984).